Primed 3D injectable microniches enabling low-dosage cell therapy for critical limb ischemia

Yaqian Li[a,b,1], Wei Liu[a,1], Fei Liu[a,c,1], Yang Zeng[a], Simin Zuo[a], Siyu Feng[d], Chunxiao Qi[a], Bingjie Wang[a], Xiaojun Yan[a], Ali Khademhosseini[e,f,g,h,i], Jing Bai[a], and Yanan Du[a,b,2]

[a]Department of Biomedical Engineering, School of Medicine, Tsinghua University, Beijing 100084, People's Republic of China; [b]Collaborative Innovation Center for Diagnosis and Treatment of Infectious Diseases, Hangzhou 310003, People's Republic of China; [c]Tsinghua–Peking Center for Life Sciences, Beijing 100084, China; [d]School of Biological Science and Medical Engineering, Beihang University, Beijing 100084, People's Republic of China; [e]Department of Medicine, Biomaterials Innovation Research Center, Brigham and Women's Hospital, Harvard Medical School, Cambridge, MA 02139; [f]Harvard–Massachusetts Institute of Technology Health Sciences and Technology, Massachusetts Institute of Technology, Cambridge, MA 02139; [g]Wyss Institute for Biologically Inspired Engineering, Harvard University, Boston, MA 02115; [h]Department of Maxillofacial Biomedical Engineering and Institute of Oral Biology, School of Dentistry, Kyung Hee University, Seoul 130-701, Republic of Korea; and [i]Department of Physics, King Abdulaziz University, Jeddah 21569, Saudi Arabia

The promise of cell therapy for repair and restoration of damaged tissues or organs relies on administration of large dose of cells whose healing benefits are still limited and sometimes irreproducible due to uncontrollable cell loss and death at lesion sites. Using a large amount of therapeutic cells increases the costs for cell processing and the risks of side effects. Optimal cell delivery strategies are therefore in urgent need to enhance the specificity, efficacy, and reproducibility of cell therapy leading to minimized cell dosage and side effects. Here, we addressed this unmet need by developing injectable 3D microscale cellular niches (microniches) based on biodegradable gelatin microcryogels (GMs). The microniches are constituted by in vitro priming human adipose-derived mesenchymal stem cells (hMSCs) seeded within GMs resulting in tissue-like ensembles with enriched extracellular matrices and enhanced cell–cell interactions. The primed 3D microniches facilitated cell protection from mechanical insults during injection and in vivo cell retention, survival, and ultimate therapeutic functions in treatment of critical limb ischemia (CLI) in mouse models compared with free cell-based therapy. In particular, 3D microniche-based therapy with 10^5 hMSCs realized better ischemic limb salvage than treatment with 10^6 free-injected hMSCs, the minimum dosage with therapeutic effects for treating CLI in literature. To the best of our knowledge, this is the first convincing demonstration of injectable and primed cell delivery strategy realizing superior therapeutic efficacy for treating CLI with the lowest cell dosage in mouse models. This study offers a widely applicable cell delivery platform technology to boost the healing power of cell regenerative therapy.

Cell-based regenerative therapy holds great promise for repair and restoration of damaged tissues or organs with numerous clinical trials and preclinical animal testing reported for treating complex diseases (1). Common route of cell administration for clinical cell therapy is based on either systematic administration (e.g., i.v. infusion), relying on cells homing to the lesion sites (2), or direct injection of cells into the damaged tissues (3). However, therapeutic benefits of the administered cells are still limited and sometimes irreproducible due to cell loss and cell death (4). Taking cell therapy for ischemic heart diseases as an example, only ~5% of mesenchymal stem cells (MSCs) survived after being transplanted into an infarcted porcine heart (5). Mechanical damage during injection, high rate of cell loss and leakage to surrounding tissues, cell death due to lack of appropriate cell–cell and cell–matrix interactions in the ischemic and inflammatory lesion tissues could all contribute to poor cell retention, survival, functionality, and reproducibility of the treatment (6, 7).

A rational solution to enhance the therapeutic efficacy and reproducibility of cell therapy is to administer a large dose of cells to ensure sufficient number of functional cells at the lesion sites. Cell dosage is a primary parameter for clinical cell therapy and in the case of bone marrow-derived mononuclear cell treatment for patients with critical limb ischemia (CLI) condition, the dose range is ~0.3 ~ 2×10^9 cells (8). There are several reports to investigate the effects of cell dosage on therapeutic outcomes in animal models (9, 10). For instance, injection of 3×10^5 MSCs exhibited no significant therapeutic angiogenesis in a mouse ischemic limb model compared with 1×10^6 MSCs, which was shown to be the minimum dosage with therapeutic effects (11).

Meanwhile, the use of a high dose of cells will not only cost more for cell processing but also bring uncontrolled risks on safety due to nonspecific cell incorporation and unwanted influence on the healthy tissues. For example, in an attempt for treating intervertebral disk degeneration, few injected MSCs were found within the intervertebral discs (IVDs) after 9 wk, whereas large anterolateral osteophytes were formed out of the IVDs that were composed of mineralized tissue surrounded by chondrocytes derived from the injected MSCs indicating potential side effect (12). The large dose of administered cells also poses higher risks of uncontrollable cell growth or even tumor genesis, especially when applying pluripotent stem cell-derived cells (13) or gene-transferred cells (14).

To improve cell retention, survival, and cell function, preformed cellular aggregates were used to replace disperse cells for injection-based therapy. However, a large amount of cells is required to preform the cell aggregates, which usually leads to high cell consumption, nonuniform size, and uncontrollable aggregate

Significance

Optimal cell delivery strategies are in urgent need to enhance the specificity, efficacy, and reproducibility of cell therapy leading to minimized cell dosage and side effects. Here, we addressed this unmet need by developing injectable 3D microscale cellular niches (microniches) based on biocompatible and biodegradable gelatin microcryogels. Dramatic improvement in cell retention, survival, and therapeutic effects enabled by the primed 3D microniches was demonstrated in treatment of critical limb ischemia (CLI) in mouse models compared with the free cell-based therapy. To the best of our knowledge, this is the first convincing demonstration of injectable and primed cell delivery strategy realizing superior therapeutic efficacy with the lowest cell dosage for treating CLI in mouse model.

MEDICAL SCIENCES

numbers (15). Moreover, cell loss in the process of aggregate formation and mechanical injury to the cells during injection are still inevitable. Alternatively, biomaterial-assisted cell delivery approaches have been developed in which responsive biomaterials (e.g., thermal or pH-sensitive hydrogel) can be coinjected with the cells in aqueous form at ambient condition and cross-linked in situ in the body to realize gelation and cell encapsulation (16). However, in situ cross-linked biomaterials such as hydrogel do not allow priming of cells, which could facilitate ECM accumulation and cell–cell interactions for construction of the cellular niche in vitro before transplantation, resulting in immediate exposure of the delivered cells to ischemic and inflammatory microenvironment at the lesion sites. Besides, in situ gelation and mechanical insult during the injection process might also cause damage to the encapsulated cells.

Clearly, there is a considerable demand for cell therapy strategies to enhance the specificity, efficacy, and reproducibility of the administered cells by improving cell engraftment, survival, and therapeutic functions precisely at the lesion sites leading to low cell dosage and minimum side effects. The need for targeted and low-dose cell therapy is analogous to its counterpart in drug-based therapy, which has been properly addressed by the maturation of drug delivery technologies.

Here, we developed injectable 3D microscale cellular niches (microniches) as optimal cell delivery and therapy vehicles to meet the abovementioned unmet need based on biocompatible and biodegradable gelatin microcryogels (GMs). The injectable 3D microniches can be constituted by in vitro priming the seeded cells in the GMs for accumulation of deposited ECM proteins as well as for enhancing cell–cell interactions. The 3D cellular microniches result in microscale tissue-like ensembles representing optimal delivery strategy to facilitate cell protection from mechanical insults during injection and in vivo cell retention, engraftment, survival, and the ultimate therapeutic functions at the lesion site. We chose CLI, one of the most advanced forms of peripheral artery disease, as a disease model to demonstrate the healing power of 3D microniche-based cell therapy. To the best of our knowledge, this is the first systematic and convincing demonstration of injectable primed 3D cell delivery strategy with superior therapeutic efficacy and the lowest cell dosage reported so far for treatment of CLI in mouse models.

Results

Fabrication and Characterization of GMs for Microscale 3D Cell Culture.
GMs were fabricated by cryogelation of gelatin within a microstencil array chip (Movie S1). The harvested GMs exhibited predefined shape and size (Fig. 1A). Interconnected macroporous structures of GMs were revealed by SEM with pore sizes in the range of 30–80 μm and porosity of $95.73\% \pm 0.28\%$ (Fig. 1B and Fig. S1A). Due to their high porosity, GMs exhibit a relatively high swelling ratio (23.49 ± 1.57) (Fig. S1A). This feature facilitates cell loading by automatic absorption of cells into GMs. Moreover, long-term preservation of the collected GMs can be realized by vacuum packaging, which can be readily delivered as an off-the-shelf product to distant users for subsequent cell culture and therapy.

We next examined the biocompatibility of GMs for microscale 3D cell culture. Human adipose-derived MSCs (hMSCs) could be automatically loaded into GMs by simply pipetting the cells onto the surface of the collected GMs. Uniform cell distribution, good cell attachment, and viability were achieved (Fig. 1C). F-actin filaments of hMSCs were also uniformly formed in GMs indicating strong cell–matrix interactions (Fig. 1D). The number of cells loaded in individual GM was controllable from 100 to 1,200 cells per GM by varying the initial cell-loading density (Fig. S1 C and D). hMSCs in GMs proliferated for at least 4 d regardless of the initial seeding densities (Fig. 1E). The initial cell seeding density of 8×10^6 cells per mL enabled rapid proliferation resulting in GMs that contained ~1,000 cells within 2 d, which was chosen for subsequent experiments.

Injectability of GMs.
GMs exhibited a Young's modulus of 8.25 ± 0.64 kPa, which could be compressed without breaking beyond the compression limit (i.e., $88.48\% \pm 2.49\%$ strain, corresponding to a stress of 61.09 ± 12.75 kPa) achievable by a Bose 3230 mechanical testing machine (Fig. S1 A and B). In contrast, gelatin hydrogel broke with $61.98\% \pm 2.75\%$ strain, corresponding to a stress of 32.86 ± 1.67 kPa. The mechanical test clearly demonstrated the excellent elasticity and deformity of GMs, indicating their great injectability as optical cell delivery vehicle compared with hydrogel. Therefore, GMs can provide shielding for cells from mechanical damage when passing through the needles during injection.

The injectability of GMs was quantitatively assessed by a programmable syringe pump integrated with a digital force gauge (7). GMs suspended in 15% (wt/vol) gelatin carrier solution could be smoothly injected and remained intact after injection. The force of injecting GMs with a density of 1,000 per mL at a flow rate of 1 mL/min was below 6 N, which was lower than the clinically acceptable force of 10 N (7) (Fig. 1F).

hMSCs in GMs could maintain high viability postinjection, indicating cell protection enabled by GMs (Fig. 1G). Moreover, hMSCs in GMs subjected to injection maintained great proliferative capacity with ~800 cells per GM on day 1 and ~1,300 cells per GM on day 5 (Fig. 1H).

Cell Priming in GMs.
As a major component of the microniches, accumulated ECMs was first investigated, which would be modulated by the priming duration and relative cell density. Expression of major ECMs was measured in hMSCs primed in GMs for 4 h and 2 d (scheme 1) and with low density and high density (scheme 2) (Fig. 2A). In scheme 1, SEM images revealed that more deposited ECMs could be observed on the surface of
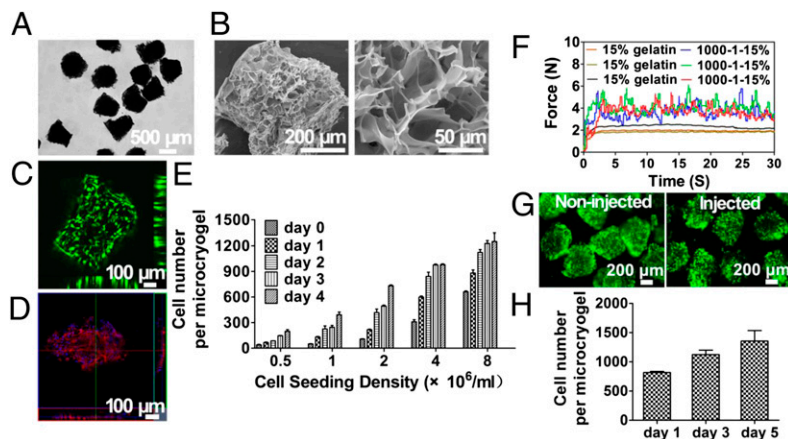

Fig. 1. Characterization of 3D injectable cellular microniches based on GMs. (A) Photographs of harvested GMs. (B) SEM images of GMs showing interconnected and macroporous structures. (C and D) Fluorescence microscopic and 3D reconstructed confocal images of GMs autoloaded with hMSCs stained by live/dead and rhodamine phalloidin. (E) Quantification of hMSCs autoloading and proliferation in GMs with different initial loading densities. (F) Real-time injection force measurement curves for triple injections of 1,000 GMs in 1 mL of 15% (wt/vol) gelatin solution at 1 mL/min injection rate (1,000–1–15%). (G) Live/dead cell viability assay of hMSCs loaded GMs preinjection and postinjection. (H) Proliferation of hMSCs loaded in GMs postinjection after 1, 3, and 5 d of culture (n = 3).

cells and macropores for hMSCs primed for 2 d compared with hMSCs primed for 4 h (Fig. 2B, *Left*). In quantitative analysis, hMSCs primed for 2 d expressed significantly higher amount of *collagen I*, *collagen IV*, and *laminin* (Fig. 2C, *Left* and Table S1) compared with those cultured for 4 h. Interestingly, gene expression of *fibronectin* was not significantly different with priming duration potentially due to the lower effectiveness of fibronectin in stimulating proliferation and differentiation of MSCs (17). In scheme 2, after 2 d of culture, SEM images revealed that high density of hMSCs deposited more ECMs on the surface of cells and macropores compared with the low density of hMSCs in GMs (Fig. 2B, *Right*). Moreover, high density of hMSCs in GMs showed significantly higher expression of *collagen I*, *collagen IV, laminin*, and *fibronectin* compared with the low-density counterpart (Fig. 2C, *Right*).

To further investigate ECM accumulation and enhanced cell–cell interaction after priming in the microniches, representative ECMs (i.e., collagen I, collagen IV, laminin, and fibronectin) and cell adhesion (i.e., E-cadherin) proteins were examined. In scheme 1, expression of collagen I, collagen IV, and laminin in hMSCs primed for 2 d was significantly higher than those primed for 4 h (Fig. 2D, *Left*), whereas expression of fibronectin between the two groups had no statistical difference, which was consistent with the gene expression data. Expression of E-cadherin in hMSCs primed for 2 d was significantly higher than that primed for 4 h. In scheme 2, high density of hMSCs in GMs expressed more collagen I, collagen IV, laminin, fibronectin, and E-cadherin than the low-density counterpart (Fig. 2D, *Right*). Expression of E-cadherin in high density of hMSCs was significantly higher compared with low density of hMSCs, indicating enhanced cell–cell interaction. These
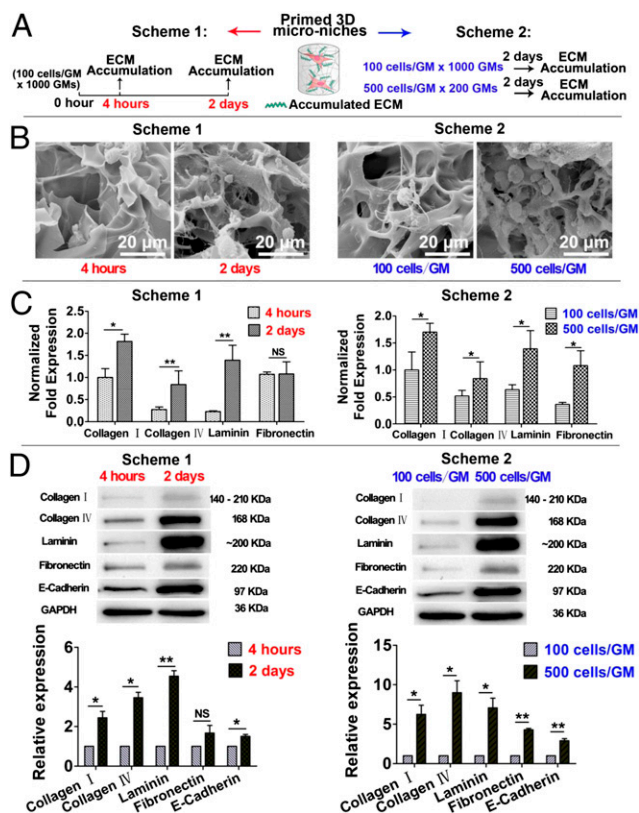
results showed that hMSCs primed for 2 d in high density might be a better priming scheme, which could accumulate abundant ECM proteins and achieve enhanced cell–cell interaction.

To investigate whether cell priming can promote therapeutic functions, hMSCs-secreted angiogenic factors (i.e., HGF and bFGF) were detected in the same two schemes. Similar to the ECM accumulation, hMSCs primed for 2 d could secrete more factors than those primed for 4 h and priming in higher density is preferred, which could significantly increase the factor secretion compared with priming in low density (Fig. S2). These results revealed that ECM accumulation and function enhancement were achieved through the priming process in GMs. More ECM expression, bioactive factor secretion from primed cells at high density indicated the importance of targeted cell delivery and retention to realize cell accumulation at the lesion sites in vivo to augment therapeutic effect.

Biodegradability of GMs and Enhanced Survival/Retention of hMSCs Microniches in Mouse Hindlimb. GMs could be degraded in the presence of trypsin/EDTA solution within 70 min (Fig. S3A). Moreover, GMs could not be detected 28 d after being injected in the intramuscular site (Fig. S3B), suggesting good biocompatibility and biodegradation in vivo.

Strong chemiluminescent signals in vivo were observed in GMs loaded with hMSCs with minimal diffusion into the surrounding tissues, whereas the signal was significantly diminished in the free-cell group 4 d after injection (Fig. 3 B and C). The difference between the two groups became more significant after 7 d. The signal was prolonged until 14 d in the mice injected with GMs loaded with hMSCs, whereas it decreased significantly in the mice injected with free cells. Semiquantifying the chemiluminescent signals within regions of interest showed that the survival rate of hMSCs in GMs was higher than free hMSCs ($96.81\% \pm 3.76\%$ vs. $15.09\% \pm 0.72\%$ on day 4; $90.44\% \pm 2.28\%$ vs. $6.13\% \pm 0.13\%$ on day 7; and $20.30\% \pm 6.57\%$ vs. $0.20\% \pm 0.02\%$ on day 14). These results indicated that the microniche-based delivery could improve hMSCs retention and survival in vivo after injection, thus benefiting their therapeutic functions.

Improved Ischemic Limb Salvage. Therapeutic efficacy of the injectable primed hMSCs microniches in limb salvage was examined by evaluating physiological status of ischemic limbs 28 d after surgery (Fig. 3A). As shown in the representative photographs and the corresponding scoring (Fig. 4 A and B and Fig. S4), no limb salvage was observed in 10^5 free-cells group ($n = 8$), GMs control group ($n = 4$), or sham group ($n = 4$). Additionally, grossly extensive forefoot necrosis was developed at 3 d after femoral artery ligation, leading to a rate of spontaneous toe amputation of three of four (75%) within 7 d in both GMs and sham groups, and finally resulted in complete limb loss for all experimental mice. The mice treated with 10^5 free cells had 50% total toe amputation, 25% partial toe amputation, and 25% partial limb amputation within 7 d, which finally resulted in 80% limb loss and 20% total toe amputation after 28 d.

In striking contrast, GMs with primed hMSCs (with total cell number of 10^5) achieved limb salvage in six of the eight (75%) mice, in which four of the six mice completely recovered their legs and the other two showed minor necrosis. Only two of the eight (25%) mice showed spontaneous toe amputation. In addition, the necrotic areas did not expand further during 28 d.

Because 10^6 hMSCs was previously reported as the minimum number for effective CLI treatment (11), it was chosen as positive control. Two of the 10^6 free hMSCs-treated mice ($n = 4$) achieved limb salvage (50%), but all had minor necrosis. One mouse showed partial toe amputation and the other one showed total toe amputation. The results further verified the superior therapeutic effects for CLI treatment achieved by the GMs+ hMSCs, which outperformed the minimum effective dosage for free cell-based therapy reported so far.

Fig. 2. Cell priming in GMs to constitute the 3D microniches. (A) Two schemes for priming hMSCs in GMs. (B) SEM images of ECMs of hMSCs in GMs under two scheme conditions. (C) Gene expression of major ECMs of hMSCs in GMs under two scheme conditions. (D) Protein expression of representative ECMs and cell adhesion protein of hMSCs under two scheme conditions. *$P <$ 0.05; **$P < 0.01$ ($n = 3$).
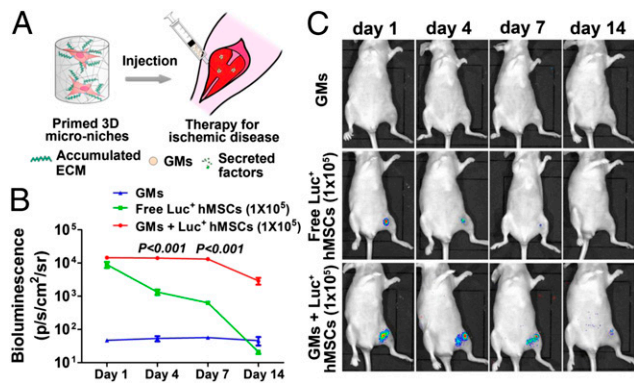
Fig. 3. Bioluminescence imaging (BLI) for tracking cell retention based on injectable GMs. (A) Schematic of the primed 3D microniches injected into the mouse hindlimb. (B) Measurement of the average radiance in standardized regions of interest from hindlimb of mice in different experiment groups on days 1, 4, 7, and 14. Luminescence signal is presented as photons per second per square centimeter per steradian (photons/s/cm²/sr). (C) BLI of mice from different groups for 1, 4, 7, and 14 d ($n = 3$).

Enhanced Angiogenesis in Ischemic Hindlimbs. More extensive microvessel formed around the ligation site of femoral artery on day 28 in the GMs+hMSCs group than the 10^5 free hMSCs group as well as other control groups (Fig. 4C). In the 10^6 free hMSCs group, sparse vessels could also be observed, but significantly less than the GMs+hMSCs group. Amazingly, the newly formed vessels in the GMs+hMSCs group could bridge the gap between the ligation sites and direct the vessel growth along the native artery.

Immunofluorescent staining and quantification for smooth muscle α-actin (SMA) (Fig. S5) demonstrated that arteriole formation in 10^5 free-cell group was comparable to the sham group. However, the arteriole formation was significantly increased in those limbs treated with GMs+hMSCs compared with those treated with 10^5 free cells. In addition, more extensive immunohistochemical staining of human nuclei antigen was observed on day 28 in limbs treated with GMs+hMSCs compared with those treated with 10^5 free cells (which was largely absent in the sham group) (Fig. S5), indicating enhanced engraftment and integration of the transplanted hMSCs in microniches with the host tissue.

Enhanced Blood Perfusion in Ischemic Hindlimb. To further evaluate therapeutic angiogenesis in vivo, indocyanine green (ICG), an angiographic contrast agent that has been Food and Drug Administration-approved for peripheral vascular imaging (18), was used as a fluorescent probe to monitor blood perfusion. A bolus of ICG was injected i.v., and dynamic fluorescence imaging was carried out immediately after injection on days 0, 3, 7, and 28 (Fig. S6 and Movies S2–S4). As shown in Fig. 5A and Fig. S7, no fluorescence signal was observed in ischemic hindlimbs of the mice in all five groups after surgery (day 0), indicating successful establishment of the ischemic models. Fluorescence signals appeared in ischemic hindlimbs of the GMs+hMSCs-treated mice around day 7, and in the 10^6 free hMSCs-treated mice since day 14. As expected, no evident fluorescence signal was observed in the ischemic hindlimbs in the sham or GMs group until day 28.

To obtain more quantitative evaluation, dynamic changes of average fluorescence intensity after ICG injection in ankle region of normal and ischemic hindlimbs are plotted simultaneously as comparison to show the healing process (Fig. 5B). Significant differences between the two curves were observed in all groups on day 0, which lasted until day 28 in the sham and GMs group. A nice correlation between the two curves was observed on day 7 in the GMs+hMSCs group, which could not be observed until day 28 in the 10^6 free hMSCs group. Meanwhile, only a slight improvement of correlation was observed in the 10^5 free hMSCs group.

These results demonstrated enhanced angiogenesis and early recovery in the GMs+hMSCs-treated ischemic hindlimbs compared with the rest of the treatment strategies. Also, cell dosage is a determining factor for the therapeutic outcome as indicated by the drastic differences between the therapeutic effects between 10^6 and 10^5 free hMSCs-treated groups.

Reduced Muscle Degeneration and Fibrosis in Ischemic Hindlimbs. H&E and Masson's trichrome staining (Fig. 4D) showed muscle degeneration and fibrosis in the ischemic regions in the sham group and GMs group on day 28. Similarly, treatment with 10^5 free hMSCs also showed large muscle degeneration and failed to maintain the large muscle fibrils observed in the normal tissue. In contrast, ischemic limbs treated with GMs+hMSCs displayed substantially reduced tissue degeneration and minimal fibrosis (Fig. 4D).

Enhanced Angiogenesis Factor Expression. Immunohistochemistry staining showed that expression of angiogenic factor (i.e., VEGF, bFGF, and HGF) in the GMs+hMSCs group could be clearly observed on day 28, whereas expression of these factors was attenuated in the 10^5 free-cell group (Fig. 6A). Likewise,
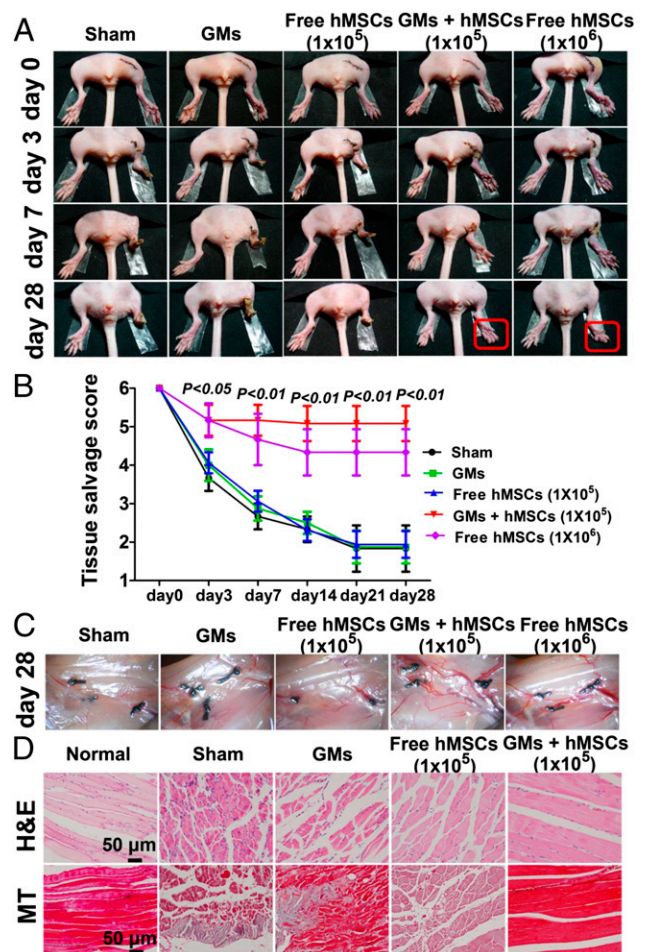

Fig. 4. Improved salvage and enhanced angiogenesis in ischemic hindlimbs based on the 3D injectable microniches. (A) Representative photographs of sham ($n = 4$), blank GMs ($n = 4$), free hMSCs (10^5) ($n = 8$), hMSCs (10^5) within GMs (GMs+hMSCs) ($n = 8$), and free hMSCs (10^6) ($n = 4$) at 0, 3, 7, and 28 d after treatment. (B) Tissue salvage sore of ischemic hindlimbs in different treatment groups. (C) Photographs showing new vessel formation across ligation sites of the ischemic hindlimbs 28 d after treatment. (D) H&E staining and Masson's trichrome staining of histological ischemic hindlimb sections 28 d after surgery. Light blue staining for collagen indicates fibrosis in Masson's trichrome staining.
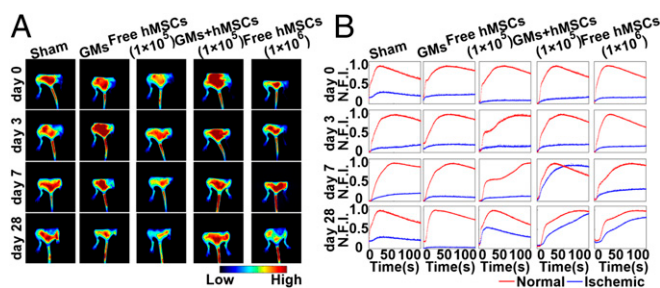
Fig. 5. Monitoring blood perfusion in ischemic hindlimb with fluorescence imaging. (*A*) Fluorescence images obtained 100 s after ICG injection on days 0, 3, 7, and 28, respectively. (*B*) Fluorescence intensity–time curves of the ankle region (indicated by the boxes in the white light images in Fig. S6; red, normal hindlimb; blue, ischemic hindlimb). Fluorescence intensities were normalized to the maximal fluorescence intensity in the ankle region of normal hindlimb. N.F.I., normalized fluorescence intensity.

quantitative analysis demonstrated significant increase in production of angiogenesis factors in the GMs+hMSCs group compared with the other three groups (Fig. 6*B*).

Discussion

Efficacy of current cell therapy for CLI is not satisfactory due to poor retention, survival, and function of the transplanted cells in the ischemic and inflammatory lesion sites with only ~3% cells being able to play a therapeutic role in the ischemic area (19). In particular, previous studies revealed the efficacy of cell therapy for CLI is dosage dependent, which usually required at least $1 \times 10^6 \sim 1 \times 10^7$ cells to exert significant therapeutic functions, and 1×10^5 cells could not effectively induce therapeutic angiogenesis in mouse models (11, 20). To improve the efficacy of cell therapy for CLI, we developed a cell delivery strategy based on primed 3D injectable microniches to achieve superior therapeutic effects for CLI with cell dosage (1×10^5 cells) 10 times less than the lowest dosage (1×10^6 cells) used in all previously reported CLI therapy.

We previously developed injectable microcryogels based on poly(ethylene glycol-diacrylate) (PEGDA) for cell delivery and preliminarily proved the enhancement of cell retention and survival after s.c. injection in mice assisted by the PEGDA microcryogels (7). Cryogel-based cell delivery has also been developed by Mooney and colleagues (21, 22), who fabricated shape-memory millimeter-scale cryogels realizing s.c. injection of a single-cell–loaded cryogel each time through a 16-gauge needle. In the present study, we developed biodegradable microscale gelatin cryogels (GMs) enabling injection of 150 GMs per mouse using clinically used setting (i.e., 23-gauge needles) for cell therapy and proved the superior therapeutic efficacy of the 3D injectable microniches by priming seeded cells within the GMs.

Accumulation of desired ECMs by cells primed in the microniche is the key factor to enhance the therapeutic effect. As the major component of native cell niches, ECMs can modulate cell behavior and fate through activating distinct signaling pathways through biophysical (e.g., surface topography and stiffness) and biochemical (e.g., growth factors, cytokines) cues (17, 23). Therefore, mimicry of natural ECMs, provide great opportunity to maximize the cell function through appropriate cell–cell and cell–matrix interaction. We believe the microcryogel-based injectable microniches developed here provide an optimal cell delivery and therapy platform that equips the cells in vitro for better therapeutic functions thanks to the priming process. The primed GMs constitute biomimetic 3D niches to accumulate ECMs [e.g., collagen I, collagen IV, laminin, and fibronectin (Fig. 2)], which can increase hMSC viability, proliferation, and differentiation to endothelial cell or smooth muscle cell (17). Moreover, the accumulated ECMs through cell priming within the microniches in vitro can increase the paracrine secretions of bioactive factors from the MSCs, such as HGF and bFGF (Fig. S2), which promote

angiogenesis at the lesion sites. In addition, thanks to the excellent elasticity and accumulated ECMs of the primed microniches based on GMs, hMSCs loaded within GMs could be shielded from the mechanical insult and necrosis during direct cell injection resulting in maintained cell viability and functionality.

After cell injection into the lesion site, another challenge is to prevent the leakage of dispersed cells to surrounding tissues and maintain cell viability and function. According to a previous study, acute (<24-h) cell retention of MSCs injected for treating ischemic diseases was normally less than 10%, regardless of the delivery route (24). In the present study, we demonstrated the importance of relative cell density at the lesion site to the overall therapeutic functions of cells with higher relative density of MSCs resulting in more ECM production and paracrine secretion of the bioactive factors (Fig. 2 and Fig. S2). Therefore, it is important to increase the relative density of cells at the lesion sites for therapy to establish stronger cell–cell and cell–ECM interactions. In this work, the primed 3D microniches could realize both long-term retention and high relative density of cells at the lesion site even when the total cell dosage was low. Therefore, the microniche-based delivery strategy greatly improves the cell–cell and cell–ECM interactions and enhances the cell survival and therapeutic functions.

Recently, several strategies such as physiological (e.g., hypoxia, heat shock) and molecular (e.g., cytokine/small molecule) treatment and genetic manipulation are investigated for stem cell preconditioning in vitro before transplantation in injured (e.g., ischemic or fibrotic) tissues (6). For example, preconditioning of hMSCs with SDF1 for 60 min was shown to enhance their ability to survive in ischemic myocardium by activation of Akt signaling pathway, resulting in reduced infarct size and left ventricular remodeling (25). Preconditioning of hMSCs with a recombinant
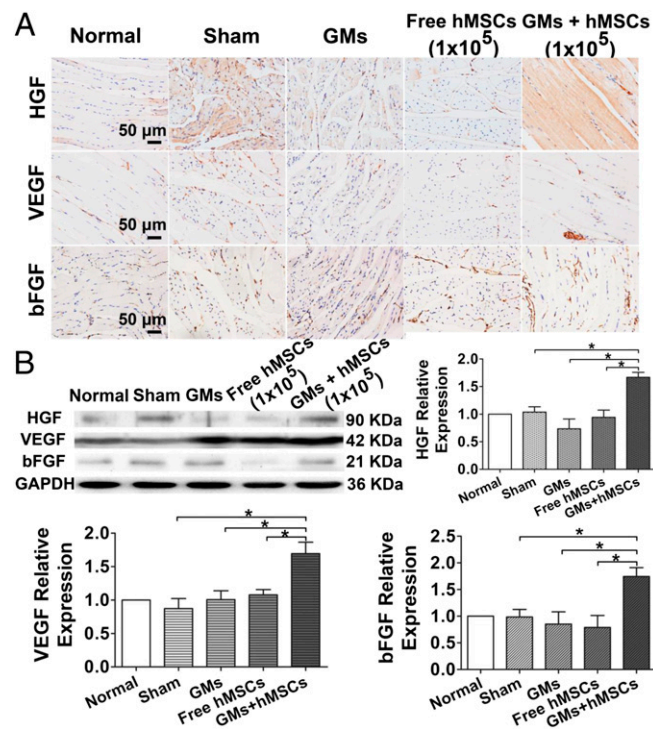

Fig. 6. Enhanced expression of angiogenic factors in ischemic hindlimbs treated with the 3D injectable microniches. (*A*) Immunohistochemical staining of ischemic muscle tissue sections 28 d after cell therapy for HGF, VEGF, and bFGF. (*B*) Images and semiquantitative analysis of Western blot for expressions of HGF, VEGF, and bFGF of ischemic muscle tissue 28 d after cell therapy. Relative expression of each protein was normalized to GAPDH, and results of each group were normalized to the result of the normal group. *$P < 0.05$ ($n = 3$).

MEDICAL SCIENCES

mixture of growth factors also led to cardiopoietic phenotype and improved their therapeutic benefit in chronic ischemic cardiomyopathy (26). In our study, effect of cell priming on hMSCs differentiation was preliminarily investigated, because up-regulated expression of ECM components was realized in the primed GMs (Fig. 2 C and D), which could direct the lineage commitment of hMSCs (17). In particular, laminin shows high affinity to bind αvβ3 integrin/CD61 receptors of hMSCs, which is critical for endothelial differentiation through activation of VEGFR and PDGFR (27). Hence we investigated the expression of *CD61* in primed hMSCs, which exhibited significantly higher expression for 2-d priming and high-density priming compared with the 4-h and low-density counterparts (Fig. S8B). We further investigated the expression of forkhead box C1 (*FOXC1*), an endothelial-specific transcriptional factor (27), and *CD31*, an endothelial marker, which showed enhanced expression of *FOXC1* for 2-d priming and high-density priming compared with the corresponding counterparts (Fig. S8C). However, no significant difference in *CD31* expression (Fig. S8D) was observed under current priming conditions (i.e., 4 h vs. 2 d; low density vs. high density), indicating that only early stage of endothelial differentiation was initiated in the primed hMSCs without full commitment to endothelial lineage. After primed for 7 d, *CD31* expression was highly up-regulated with significant increase compared with 2-d priming, indicating that the primed hMSCs could differentiate into endothelial lineage after a longer term of priming.

Timing for hMSCs priming is a critical parameter to consider for optimal therapeutic efficacy. As hMSCs may become senescent (e.g., morphology alteration, declined differentiation potential, and progressive growth arrest) during long-term culture/expansion in vitro (28), there exists a balance between the benefits in ECM/bioactive factor accumulation and the potential cell

senescence during cell priming. Systematic investigation and optimization on the priming timing and its influence on cell fate and therapeutic efficacy of CLI treatment will be the focus of our future study, which is expected to be vital to fully release the therapeutic power in regenerative medicine. Meanwhile, we will explore the possible mechanism and ultimate fate of the transplanted cells by tracking the cell location, migration, and differentiation at the lesion site.

The ultimate goal of regenerative medicine is to achieve targeted and high-efficient therapy with minimum dosage and side effects of the administered cells. It is envisioned that the microniche-assisted cell therapy system holds great promise to realize this goal as a widely adopted platform technology.

Materials and Methods

Detailed information is provided in *SI Materials and Methods*.

GMs (with diameters of 400 μm) were prepared by a microstencil array chip (75 cm × 25 cm with thickness of 300 μm) (29). Briefly, 6% (wt/vol) gelatin precursor solution was mixed with 0.3% glutaraldehyde, and then 200 μL of precursor solution was pipetted and scraped onto the microstencil array chip. The microstencil array chip underwent cryogelation for 16 h and then was lyophilized for 30 min (Boyikang). GMs were then harvested by a PMMA Ejector Pin array fabricated by a desktop 3D milling machine (MDX-40A; Roland DG) (9).

1. Gimble JM, Guilak F, Bunnell BA (2010) Clinical and preclinical translation of cell-based therapies using adipose tissue-derived cells. *Stem Cell Res Ther* 1(2):19.
2. Sheikh AY, et al. (2007) Molecular imaging of bone marrow mononuclear cell homing and engraftment in ischemic myocardium. *Stem Cells* 25(10):2677–2684.
3. Amado LC, et al. (2005) Cardiac repair with intramyocardial injection of allogeneic mesenchymal stem cells after myocardial infarction. *Proc Natl Acad Sci USA* 102(32):11474–11479.
4. Cheng AY, García AJ (2013) Engineering the matrix microenvironment for cell delivery and engraftment for tissue repair. *Curr Opin Biotechnol* 24(5):864–871.
5. Freyman T, et al. (2006) A quantitative, randomized study evaluating three methods of mesenchymal stem cell delivery following myocardial infarction. *Eur Heart J* 27(9):1114–1122.
6. Thai HM, et al. (2009) Implantation of a three-dimensional fibroblast matrix improves left ventricular function and blood flow after acute myocardial infarction. *Cell Transplant* 18(3):283–295.
7. Liu W, et al. (2014) Microcryogels as injectable 3-D cellular microniches for site-directed and augmented cell delivery. *Acta Biomater* 10(5):1864–1875.
8. Lawall H, Bramlage P, Amann B (2010) Stem cell and progenitor cell therapy in peripheral artery disease. A critical appraisal. *Thromb Haemost* 103(4):696–709.
9. Zhang L, et al. (2011) Delayed administration of human umbilical tissue-derived cells improved neurological functional recovery in a rodent model of focal ischemia. *Stroke* 42(5):1437–1444.
10. Kim H, et al. (2010) Dose-dependent efficacy of ALS-human mesenchymal stem cells transplantation into cisterna magna in SOD1-G93A ALS mice. *Neurosci Lett* 468(3):190–194.
11. Kinnaird T, et al. (2004) Local delivery of marrow-derived stromal cells augments collateral perfusion through paracrine mechanisms. *Circulation* 109(12):1543–1549.
12. Vadalà G, et al. (2012) Mesenchymal stem cells injection in degenerated intervertebral disc: cell leakage may induce osteophyte formation. *J Tissue Eng Regen Med* 6(5):348–355.
13. Seminatore C, et al. (2010) The postischemic environment differentially impacts teratoma or tumor formation after transplantation of human embryonic stem cell-derived neural progenitors. *Stroke* 41(1):153–159.
14. Hacein-Bey-Abina S, et al. (2003) A serious adverse event after successful gene therapy for X-linked severe combined immunodeficiency. *N Engl J Med* 348(3):255–256.
15. Moreira Teixeira LS, et al. (2012) High throughput generated micro-aggregates of chondrocytes stimulate cartilage formation in vitro and in vivo. *Eur Cell Mater* 23:387–399.

16. Ifkovits JL, et al. (2010) Injectable hydrogel properties influence infarct expansion and extent of postinfarction left ventricular remodeling in an ovine model. *Proc Natl Acad Sci USA* 107(25):11507–11512.
17. Kuraitis D, Giordano C, Ruel M, Musarò A, Suuronen EJ (2012) Exploiting extracellular matrix-stem cell interactions: a review of natural materials for therapeutic muscle regeneration. *Biomaterials* 33(2):428–443.
18. Kang Y, et al. (2009) Quantitative analysis of peripheral tissue perfusion using spatiotemporal molecular dynamics. *PLoS One* 4(1):e4275.
19. Laflamme MA, Murry CE (2005) Regenerating the heart. *Nat Biotechnol* 23(7):845–856.
20. Mima Y, et al. (2012) Enhancement of cell-based therapeutic angiogenesis using a novel type of injectable scaffolds of hydroxyapatite-polymer nanocomposite microspheres. *PLoS One* 7(4):e35199.
21. Bencherif SA, et al. (2012) Injectable preformed scaffolds with shape-memory properties. *Proc Natl Acad Sci USA* 109(48):19590–19595.
22. Koshy ST, Ferrante TC, Lewin SA, Mooney DJ (2014) Injectable, porous, and cell-responsive gelatin cryogels. *Biomaterials* 35(8):2477–2487.
23. Lin H, Yang G, Tan J, Tuan RS (2012) Influence of decellularized matrix derived from human mesenchymal stem cells on their proliferation, migration and multi-lineage differentiation potential. *Biomaterials* 33(18):4480–4489.
24. Cheng K, et al. (2010) Magnetic targeting enhances engraftment and functional benefit of iron-labeled cardiosphere-derived cells in myocardial infarction. *Circ Res* 106(10):1570–1581.
25. Pasha Z, et al. (2008) Preconditioning enhances cell survival and differentiation of stem cells during transplantation in infarcted myocardium. *Cardiovasc Res* 77(1):134–142.
26. Behfar A, et al. (2010) Guided cardiopoiesis enhances therapeutic benefit of bone marrow human mesenchymal stem cells in chronic myocardial infarction. *J Am Coll Cardiol* 56(9):721–734.
27. Wang CH, Wang TM, Young TH, Lai YK, Yen ML (2013) The critical role of ECM proteins within the human MSC niche in endothelial differentiation. *Biomaterials* 34(17):4223–4234.
28. Izadpanah R, et al. (2008) Long-term in vitro expansion alters the biology of adult mesenchymal stem cells. *Cancer Res* 68(11):4229–4238.
29. Li X, et al. (2014) Micro-scaffold array chip for upgrading cell-based high-throughput drug testing to 3D using benchtop equipment. *Lab Chip* 14(3):471–481.